



Pan, X., Yu, Q., You, Y., Chun, K. P., Shi, X. and Li, Y. (2017)  
Contribution of supra-permafrost discharge to thermokarst lake water  
balances on the northeastern Qinghai-Tibet Plateau. *Journal of Hydrology*,  
555, pp. 621-630. (doi:[10.1016/j.jhydrol.2017.10.046](https://doi.org/10.1016/j.jhydrol.2017.10.046))

This is the author's final accepted version.

There may be differences between this version and the published version.  
You are advised to consult the publisher's version if you wish to cite from  
it.

<http://eprints.gla.ac.uk/174220/>

Deposited on: 27 November 2018

Enlighten – Research publications by members of the University of Glasgow  
<http://eprints.gla.ac.uk>

# Accepted Manuscript

Research papers

Contribution of supra-permafrost discharge to thermokarst lake water balances on the northeastern Qinghai-Tibet Plateau

Xicai Pan, Qihao Yu, Yanhui You, Kwok Pan Chun, Xiaogang Shi, Yanping Li

PII: S0022-1694(17)30721-7

DOI: <https://doi.org/10.1016/j.jhydrol.2017.10.046>

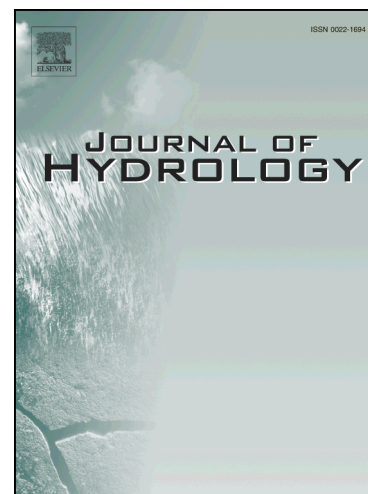
Reference: HYDROL 22326

To appear in: *Journal of Hydrology*

Received Date: 29 May 2017

Revised Date: 20 October 2017

Accepted Date: 21 October 2017



Please cite this article as: Pan, X., Yu, Q., You, Y., Pan Chun, K., Shi, X., Li, Y., Contribution of supra-permafrost discharge to thermokarst lake water balances on the northeastern Qinghai-Tibet Plateau, *Journal of Hydrology* (2017), doi: <https://doi.org/10.1016/j.jhydrol.2017.10.046>

This is a PDF file of an unedited manuscript that has been accepted for publication. As a service to our customers we are providing this early version of the manuscript. The manuscript will undergo copyediting, typesetting, and review of the resulting proof before it is published in its final form. Please note that during the production process errors may be discovered which could affect the content, and all legal disclaimers that apply to the journal pertain.

**Contribution of supra-permafrost discharge to thermokarst lake water balances on the northeastern Qinghai-Tibet Plateau**

Xicai Pan<sup>1</sup>, Qihao Yu<sup>2</sup>, Yanhui You<sup>2</sup>, Kwok Pan Chun<sup>3</sup>, Xiaogang Shi<sup>4</sup>, and Yanping Li<sup>5</sup>

<sup>1</sup> Fengqiu Agro-ecological Experimental Station, State Key Laboratory of Soil and Sustainable Agriculture, Institute of Soil Science, Chinese Academy of Sciences, Nanjing, China

<sup>2</sup> State Key Laboratory of Frozen Soils Engineering Cold and Arid Regions Environmental and Engineering Research Institute, Chinese Academy of Sciences, Lanzhou, China

<sup>3</sup> Department of Geography, Hong Kong Baptist University, Hong Kong, China

<sup>4</sup> Lancaster Environment Centre, Lancaster University, Lancaster, United Kingdom

<sup>5</sup> Global Institute for Water Security, University of Saskatchewan, Canada

*Correspondence to: X. Pan (xicai.pan@issas.ac.cn)*

**Abstract**

The seasonal hydrological mechanisms of two thermokarst lakes on the northeastern Qinghai-Tibet Plateau (QTP) were characterized by three-year intensive field observations and a water balance model. In three ice-free seasons, the supra-permafrost discharge contributed a mean ratio of over 170% of the precipitation. In the ice-cover seasons, the supra-permafrost discharge contribution varied between -20% and 22% of the water storage change. Results show that a large portion of the lake water storage change is because of the supra-permafrost discharge resulting from precipitation. Furthermore, a precipitation-subsurface runoff function is preliminarily identified in which the supra-permafrost discharge nonlinearly increased with more precipitation. Our results show that the recent lake expansion is linked with increasing supra-permafrost discharge dominated by precipitation. This study also suggests that we need to pay attention to the nonlinear increase of precipitation-controlled supra-permafrost discharge on the large lake expansion at the catchment scale in the QTP region, instead of only looking at the inputs (e.g., precipitation and river discharge) as shown in the previous studies.

## 1 Introduction

Thermokarst lakes are typically formed by the settlement of ground following thawing of ice-rich permafrost or melting of massive ice (van Everdingen, 2005). They are widely distributed throughout the pan-Arctic lowlands (Smith et al., 2005) and also occur in alpine permafrost, such as mountain valleys and plateaus (e.g., Kaeab and Haeberli, 2001; Harris, 2002; Niu et al., 2011). Thermokarst lakes do not only affect the continuity of permafrost (Burn, 2002) but are also important for the land-atmosphere energy exchange (Rouse et al., 2003) and the carbon cycle (Kling, 1991; Zimov, 1997), aquatic ecology and migratory birds (Vincent and Hobbie, 2000). Coincident with global increasing temperature, local warming would lead to abrupt environmental shifts such as rapid hydro-geomorphic changes (e.g. Arp et al., 2011) and accelerated greenhouse gases releases (Walter et al., 2006). Therefore, understanding the mechanism of thermokarst lake evolution is essential for abrupt change adaptations in the cold regions. Compared to the relatively abundant research on thermokarst lakes in the pan-Arctic, our understanding of the thermokarst lakes on the Qinghai-Tibet Plateau (QTP) is far less.

Given different hydro-meteorological conditions, the hydrological and thermal regimes of thermokarst lakes are different between the Arctic and the QTP. In the Arctic, the annual lake water storage change is mainly controlled by precipitation, evaporation, surface runoff induced by spring snowmelt and rainfall, and subsurface runoff induced by ground-ice thawing and infiltrated water (Bowling et al., 2003; Pohl et al., 2009). Since snowmelt runoff dominates the annual runoff contribution (McNamara et al., 1998), the major factors of the presence of permafrost, topography, the antecedent hydrologic processes (precipitation, evapotranspiration, and soil moisture) are essential to lake water balance. The subsurface flow affected by rainfall, active layer thaw only take place in the tundra region with a relatively

thick organic layer (Quinton and Marsh, 1999). In contrast, thermokarst lakes in the northeastern QTP have a different weather condition because summer rainfall is a major input, and snowmelt is rather small due to little snowfall. As a result, subsurface runoff can be very important to the lake water balance, and the factors affecting the precipitation-runoff mechanism like rainfall intensity and duration, soil hydraulic properties, active layer thaw should be addressed.

It is widely recognized that the permafrost degradation affects the hydrological cycles in high latitude or altitude environments, but the relationship between permafrost degradation and the change of streams, rivers, and lakes are still debated. Generally, permafrost degradation would result in lake expansion due to releasing meltwater and increasing contributing area of the lake watershed (e.g., Connon et al., 2014). Besides, thawing permafrost will lead to more water being routed through subsurface pathways and will increase groundwater storage capacity. Therefore, the increase of hydrologic and hydrogeologic connectivity of landscapes might lead to lake expansion (Walvoord and Kurylyk, 2016). Therefore, the changing precipitation could interact with the water distribution over different attitudes and these complex relationships on the QTP should be further studied. For example, Lei et al. (2013) quantitatively assessed the water balances of six closed lakes in the central QTP for the period 1976-2010, and found that the increased precipitation and runoff, and decreased lake evaporation were the main causes for the coherent lake growth, and their contribution was much higher than the accelerated glacier discharge. Similar causes were suggested by Song et al. (2014) through qualitatively analyzing the relationship between the water-level changes of lakes and the potential drivers over the whole plateau in the 2000s. Zhou et al. (2015) did a thorough exploration of the water storage changes of the largest lake (Selin Co) for a period of 2003-2012 and found that the contribution of lake inflows accounts for 49.5% for the lake growth, while precipitation

and evaporation over the lake collectively account for 40.4%. However, the precipitation-runoff (surface and subsurface) mechanism, controlled by permafrost was seldom addressed in these studies.

In this study, we characterized the hydrological mechanism of two shallow thermokarst lakes on the northeastern QTP, by intensive field-observations over three years and a water balance model. The specific objectives are to: (1) quantify the contribution of supra-permafrost discharge to the lake water balance through a water balance with the supra-permafrost flow contribution treated as a residual term; and (2) conceptualize the precipitation-runoff mechanism. To be an alternative method of the stable water isotope tracing (e.g., Gibson, 2001; Brock et al., 2007; Labrecque et al., 2009; Turner et al., 2010; Yang et al., 2016), the direct water balance quantification in this study cannot only infer the hydrological mechanism of the thermokarst lakes, but also can provide new insights for interpreting the lake growth trends on the QTP.

## **2 Site description and instrumentation**

The study site is located at 35°11'N, 93°57'E with an elevation of 4445 m a.s.l. (above sea level) in the north-eastern QTP, China (Fig. 1). It lies on the riverbank of the Chumaer River on the Chumaer High Plain. Permafrost in this area consists of a thick active layer (> 2 m) and underlying ice-rich permafrost with a thickness of 20–30 m (Zhou et al., 2000). The terrain is gently sloping to the river, and a large amount of small and shallow thermokarst lakes spread in this region (Niu et al., 2011).

Two small thermokarst lakes (Lake A and Lake B Fig. 1b), a few kilometers from the Chumaer River, were selected to investigate their hydrological dynamics. Both of them are rectangular in shape, and they gently slope towards the river valley in the north. The open-water areas of Lake A and Lake B are about 6000 m<sup>2</sup> (50m×120m) and 15400 m<sup>2</sup>

(70m×220m), respectively. Lake A is relatively isolated to other lakes, while Lake B is intermittently connected to the other lakes via a trail (dashed line in Fig. 1b), which could be a hydrologic conduit when the lake overflows. These lakes in this region are usually ice-free for a half of the year, and they may freeze to the bottom due to their shallow water depths (less than 2 meters) (Niu et al., 2011).

The hydrological conditions of the two lakes have been studied before. Using borehole temperatures and Electrical Resistivity Tomography sounding, You et al., (2017a) found that there is no permafrost underlying Lake A, which means a through talik. In addition to the annual expansion-shrinking cycle, the lake has been slowly expanding due to lateral thermal erosion by supra-permafrost water flow (You et al., 2017b). The borehole drilling around the lakes shows that the strata consist of a surficial layer of sandy loam and gravel (2-2.5 m) and a thick layer of weathered mudstone, over 20 m. For the coarse soil of the upper layer, the supra-permafrost discharge is significant in the lake water dynamics (Pan et al., 2014). Although the lakes connect to the sub-permafrost aquifer, the lake seepage through the thick and low permeable lacustrine deposits is rather small according to the borehole drilling. Therefore, the lake water dynamics are mainly controlled by the land surface processes and supra-permafrost lateral flows, but not by the vertical thorough flows.

An automate soil-weather monitoring station was located close to the lakes. A detailed description of the instrumentation can be found in Pan et al. (2016). Meteorological data from 2007 to 2011 shows mean annual air temperature was  $-4.0^{\circ}\text{C}$  and the mean annual precipitation about 300 mm (Pan et al., 2014). Observations from the weather stations show only 2.3% of precipitation occurred as snow in winter from 1962 to 2004 in this region (Li et al., 2006). The rainy season mainly occurs between June and September, and a thin snow cover usually appears on land before and after the rainy season.

Lake water-level and bottom temperature dynamics at the two lakes were monitored using two water level loggers (HOBO U20 Water Level Data Logger, Onset Computer Corporation). They were put on the lake floor in a deep area, where the water depths at that time were 65 cm and 58 cm at Lake A and Lake B, respectively. The water levels were both monitored with an interval of one hourly at the beginning, but the logger at Lake A was set to take measurements every two hours since October 26, 2013. In addition, monitoring of the supra-permafrost water level at borehole B0 on the northern bank of Lake A was initiated on October 31, 2012. A level logger was deployed at a depth of 1.56 m, which was about 20 cm below the supra-permafrost water level on that day. These recorders have a typical accuracy of 0.5 cm for water head measurements, as is specified by the manufacturer of the instrument.

### 3 Methods

#### 3.1 Seasonal water balance

For understanding the seasonal difference, two water budgets were performed in each hydrological year at the two lakes. One is for the ice-free season and the other one is for the ice-cover season. Components of lake water balance mainly include precipitation, surface-subsurface lateral inflow, evaporation/sublimation, vertical seepage, and surface-subsurface lateral outflow. A general lake water balance is expressed as

$$P - E + \Delta L + Q_s = \Delta S \quad (1)$$

where,  $P$  is direct precipitation (including solid and liquid forms) to the lake,  $\text{mm d}^{-1}$ ,  $E$  is actual evaporation/sublimation,  $\text{mm d}^{-1}$ ,  $\Delta L$  is net lateral water flux consisting of both surface and subsurface runoff,  $\text{mm d}^{-1}$ ,  $Q_s$  is lake water seepage,  $\text{mm d}^{-1}$ , and  $\Delta S$  is the lake water volume change,  $\text{mm d}^{-1}$ . For the two lakes, lake water seepage through the low permeability mudstone was assumed negligible. Therefore, the water balance Eq. (1) is simplified as

$$P - E + \Delta L = \Delta S \quad (2)$$

where,  $P$ ,  $E$ , and  $\Delta S$  are calculated from field observations, but  $\Delta L$  is unknown.

The ice-cover period is between the freeze-up date and the break-up date, which it is usually determined by in-situ identification or remote sensing (e.g., Livingstone, 1999; Kouraev et al., 2007). However, the in-situ freeze-up and break-up dates are not available for the study sites. We defined the freeze-up and break-up dates based on air temperatures and lake bottom temperatures. During the ice-free season, there is no thermal stratification of the QTP thermokarst lakes because of turbulent mixing in their shallow water bodies (Niu et al., 2011). However, during the early ice-cover season, the emergence of ice cover would reduce the lake water temperature variations below the ice cover. Consequently, the diurnal range of lake bottom temperature also decreases in the early ice-cover. As illustrated in Fig 2b, a clear transition of the diurnal amplitude of the lake bottom temperature occurs at the end of the ice-free season. Similarly, the transition can be found at the end of the ice-cover season, although there are some abnormal measurements at the end of the ice-cover season. In this study, we define the freeze-up date to be the day with a maximum air temperature of zero degree along with a clear seasonal decrease of the daily amplitude of the lake bottom temperature. Similarly, we define the break-up date as the day with a mean air temperature of zero degree along with a clear seasonal increase of the daily amplitude of the lake bottom temperature. Thus, the gray areas in Fig. 2 show the two ice-cover seasons between 2012 and 2014: (1) from October 15 2012 to April 20, 2013, and (2) from October 16, 2013 to May 4, 2014. These periods are consistent with the field observations of ice formation at the thermokarst lakes on the northeastern QTP (Lin et al., 2010; Niu et al., 2011).

### 3.2 Estimating lake evaporation/sublimation

The lake evaporation  $E$  was estimated separately as open-water evaporation  $E_t$  for the ice-free season and sublimation  $E_f$  for the ice-cover season. The open-water evaporation  $E_t$  is commonly determined with physical models. There are a wide variety of methods such as mass balance, energy budget models, bulk transfer models, combination models, equilibrium temperature methods and empirical approaches (e.g. Finch and Calver, 2008; McMahon et al., 2013). However, there is no generally accepted best method and different evaporation models often give different estimations (Finch and Hall, 2001). In practice, method selection usually relies on the data availability and quality. Given the limited measurements of lake water temperature, the straightforward approaches using a lake surface energy balance are not viable for the studied case. Concerning the open water with a depth less than 2.0 m, an alternative approach suggested by the FAO (Allen et al., 1998) was used by combining a terrestrial method and a coefficient  $K_w$  as

$$E_t = K_w ET_0 \quad (3)$$

The reference evapotranspiration  $ET_0$  was calculated based on available measurements from the automatic weather station nearby the lakes, and a value of 1.05 for the coefficient  $K_w$  was used as suggested by FAO-56 for the shallow lake with a depth of less than 2 m. The reference evapotranspiration  $ET_0$  mm d<sup>-1</sup> is calculated using the Penman-Monteith method (Allen et al., 1998). The equation is

$$ET_0 = \frac{0.408\Delta(R_n - G) + \gamma \frac{900}{T_a + 273} u(e_s - e_a)}{\Delta + \gamma(1 + 0.34u_2)} \quad (4)$$

where,  $R_n$  is net radiation, MJ m<sup>-2</sup> d<sup>-1</sup>;  $G$  is soil heat flux density, MJ m<sup>-2</sup> d<sup>-1</sup>;  $T_a$  is daily mean air temperature, °C;  $u$  is daily mean wind speed at 2-m height, m s<sup>-1</sup>;  $e_s$  and  $e_a$  are saturated and

actual vapor pressure, respectively, kPa;  $\Delta$  is slope vapor pressure curve, kPa  $^{\circ}\text{C}^{-1}$ ;  $\gamma$  is psychometric constant, kPa  $^{\circ}\text{C}^{-1}$ . Calculation of corresponding atmospheric items is listed in Table 1.

Soil heat flux density  $G$  in Eq. (4) was determined by measuring the total thermal energy change in the active layer. The total energy including sensible heat and latent heat can be calculated from soil temperature and water content measurements in the active layer. The latent heat of fusion from solid to liquid was determined from the measured unfrozen water content and ice content, and the latter one was calculated using the pre-freeze soil water content minus the measured unfrozen water content. Here, an areal density  $E_g$  was used to represent the stored energy in the active layer. In this study, the active layer is defined to be between the surface and a reference depth  $z_r$  (2.28 m), which was the deepest soil water content sensor close to permafrost table.  $E_g$  was calculated from the reference state where the soil is assumed to be at zero temperature.

$$E_g(t) = \sum_{\alpha \in \{s,w,i\}} c_{\alpha} \rho_{\alpha} \int_0^{z_r} \theta_{\alpha}(z,t) T(z,t) dz - L_{sf} \rho_i \int_0^{z_r} \theta_i(z,t) dz \quad (5)$$

where,  $s, w, i$  are indices of soil matrix, unfrozen water and ice;  $c_{\alpha}$  is specific heat of the materials (0.733, 0.422, 2.11, MJ  $\text{kg}^{-1} \text{K}^{-1}$ , respectively);  $\rho_{\alpha}$  is density of the materials ( $2.65 \times 10^3$ ,  $1.0 \times 10^3$ ,  $0.917 \times 10^3$   $\text{kg m}^{-3}$ , respectively);  $L_{sf}$  is latent heat of ice fusion from solid to liquid, 0.33 MJ  $\text{kg}^{-1}$ ;  $\theta_{\alpha}$  is volumetric content of each phases,  $\text{m}^3 \text{m}^{-3}$ .

Given the deep reference depth with negligible heat flux below it, surface soil heat flux density  $G$  is calculated by

$$G(t) = \frac{\partial E_g(t)}{\partial t}. \quad (6)$$

Estimating sublimation  $E_f$  is challenging due to limited knowledge for winter sublimation (Liston and Sturm, 2004). In the pan-arctic, sublimation can be up to 50% of the total winter precipitation due to the strong blowing snow (e.g., Sturm et al., 2001; Pomeroy and Essery, 1999), but winter snow sublimation on the QTP is insignificant because the amount of snowfall is rather small. But lake ice sublimation may not be negligible. Thus, for the ice-cover season, the sublimation was roughly estimated with the aerodynamic method in this study. The daily sublimation  $E_f$ ,  $\text{mm d}^{-1}$ , is determined as the product of an empirical wind function and the atmospheric saturation deficit between the evaporating surface and the overlying atmosphere (Kuchment and Gelfan, 1996)

$$E_f = 3.282 \cdot (0.18 + 0.098u)(e'_s - e_a) \cdot 8.64 / L_{sv}, \quad (7)$$

where  $L_{sv}$  is the sublimation heat of ice ( $2.834 \text{ MJ kg}^{-1}$ ), and the saturation vapor pressure over ice surface  $e'_s$ , kPa, is calculated by

$$e'_s = 0.6112 \exp \left[ \frac{2.834 \times 10^6}{461.5} \left( \frac{1}{273.16} - \frac{1}{T_a} \right) \right]. \quad (8)$$

The uncertainty of the estimations of the lake evaporation and sublimation ( $E_t$ ,  $E_f$ ) originate from the error of meteorological measurements (typically around  $\pm 5\%$ ) and the model error, namely, improper evaporation/sublimation model presentation. For  $E_t$ , it is mainly affected the empirical factor  $K_w$ , which is sensitive to water depth (Finch and Calver, 2008). For  $E_f$ , it is mainly affected by the empirical wind function, since it was derived from snow surface rather lake ice surface. On average, an error of 15% was approximated in these seasonal estimations  $E_t$  and  $E_f$ .

### 3.3 Rainfall estimation through soil water content observations

Snow precipitation observations were not available, but snow cover can be roughly inferred from observations of distance change from an acoustic sensor. Considering a few light snowfall events, they were neglected in Eq. (2). Rain precipitation was measured with a tipping bucket rain gauge. However, the monitoring of rainfall by tipping bucket rain gauges in remote and harsh fields suffers from limitations, i.e., disturbances by bird drop, and data gaps due to instrument malfunction. Therefore, an alternative approach using near-surface soil moisture is preferable considering the robustness of field measurements (e.g., Brocca et al., 2013). This method employs a simplified water balance for a shallow layer depth, including precipitation, fluctuation rate of soil water storage and downward drainage rate

$$p(t) \approx Z \frac{\partial s(t)}{\partial t} + as(t)^b, \quad (9)$$

where,  $P$  is estimated rainfall,  $\text{mm d}^{-1}$ ;  $Z$  is the water capacity of the soil layer,  $\text{mm}$ ;  $a$  and  $b$  are the parameters of the drainage rate,  $\text{mm d}^{-1}$  and dimensionless, respectively;  $s(t)$  is the measured relative saturation of the soil;  $t$  is time,  $\text{d}$  (day). For a specific site, the parameters ( $Z$ ,  $a$  and  $b$ ) can be estimated through calibration. Excellent performances of this approach have been demonstrated at sites over a range of climates and locations in Europe (Brocca et al., 2015).

In this study, daily rainfall rates were estimated with the above-mentioned approach by using soil water content measurements at a depth of 10 cm near the surface. The porosity of the sandy loam soil is 0.4. Using a fourth-order Runge-Kutta scheme for the discrete form of Eq. (9), the parameters were solved by minimizing the measured relative soil saturation values in the first ice-free season (June 29 to October 14 in 2012). Results in Fig. 3a show a satisfactory correlation coefficient ( $R = 0.69$ ) between observed and estimated daily rainfall

rates. However, it is known that this type of methodologies based on soil moisture data for estimating or correcting rainfall usually underestimates the total rainfall amount, and the bias depends on the soil saturation (Brocca et al., 2015). Given the observed saturation in Fig. 3b, we estimated the standard error of the mean difference between observed and estimated values by a bootstrap method (Efron and Tibshirani, 1993). The estimated standard error of the mean is  $0.35 \text{ mm d}^{-1}$ . The bias of underestimation reached an average of -21%, which is within the reported bias range by Brocca et al. (2015). The subsequent ice-free seasons were all directly calculated using the calibrated parameters ( $Z = 216 \text{ mm}$ ,  $a = 12.0 \text{ mm d}^{-1}$  and  $b = 3.39$ ), and their uncertainties were assumed to be the same as the calibration period.

### 3.4 Lake water volume change

Lake water volume change in ice-free season was determined from water level observations. It is measured by the absolute pressure difference between water pressure and atmospheric pressure from water level loggers. The atmosphere pressures used in this study were corrected from measurements from a weather station in the same region (Beiluhe, 4630 m a.s.l.), since the barometer malfunctioned at the site. Overall, the accuracy of water level is around 5 mm according to the sensor specification by the manufacturer. Here we note that the effect of lake topography on water budget was often neglected as in typical lake water balance models (Hayashi and van der Kamp, 2007; Finch and Calver, 2008).

For the ice-cover season, the above calculation for water level can be valid at the beginning and the end of the period due to the connection of lake water to atmosphere via active layer surrounding the lake edge. However, the sensors cannot be used in freezing soils, and this leads to data gaps of the water level measurements in Fig. 4b.

### 3.5 Determining the supra-permafrost discharge

The flow paths of surface and subsurface runoff varied in time in space, making it difficult to directly measure the net lateral water flux  $\Delta L$ . In this study,  $\Delta L$  was determined as the residual of other water balance components from Eq. (2)

$$\Delta L = \Delta S - P + E .$$

(10)

Since surface runoff was negligible in this gentle plain with high permeable soils and little snow melt water, Lake A is a water-closed system. While Lake B is approximately water-closed except that sporadic intermittent runoff might occur through the trail when extreme precipitation happens. Generally,  $\Delta L$  is dominated by the supra-permafrost discharge, which could be inferred from direct observations of water levels of the supra-permafrost aquifer and the lakes.

The uncertainty of the supra-permafrost discharge  $\Delta L$  is dependent on the errors in  $P$ ,  $E$ , and  $\Delta S$  in Eq. (10). The uncertainties in  $P$  and  $E$  represent cumulative errors, and the uncertainty in  $\Delta L$  means point-in-time error between the beginning and end of each season. For the ice-free season, errors in these three inputs were considered. But only the first two were included for the ice-cover period, because snow precipitation was assumed to be zero. Generally, the uncertainty for  $\Delta L$  was represented by the estimated by the 95% confidence intervals estimated from a root mean squared sum of the errors of water balance components in Eq.

(10).

## 4 Results and discussion

### 4.1 Lake water balance and seasonal supra-permafrost discharge estimations

The hydrological conditions over the years 2012-2014 are shown in Fig. 4, and the quantified water balance components for each season are presented in Table 2. The daily mean air temperature ranged from -23.5 to 13.0°C, and the active layer experienced seasonal freeze-thaw cycles down to a depth of around 2.4 m. The precipitation was concentrated in the ice-free season, and was negligible in the ice-cover season. As a result, the water level of the lakes was significantly elevated by rainfall in the ice-free season and decreased gradually in the ice-cover season. The corresponding contribution of the supra-permafrost discharge is summarized as follows.

In the ice-free season, the water level dynamics of the lakes were strongly correlated with rainwater. The rapid rises of the lake water levels are consistent with the rising supra-permafrost water level in the seasons of 2013 and 2014. The supra-permafrost discharge in the three ice-free seasons ranged from 194 mm to 667 mm, with a mean of 407 mm at Lake A, with a smaller mean discharge of 362 mm at Lake B. The difference is attributed to the size of the open areas of the two lake systems. Lake A is rather disconnected, but surface runoff goes into Lake B if the water level is over a certain threshold.

During the ice-cover season, the contribution of the supra-permafrost discharge to lake water volume change was not negligible before freezing up of the active layer. Without direct observations of the lake water volume changes, the water storage changes were deducted from the beginning and the end of the ice-cover season. From 2012 and 2013, the supra-permafrost discharge estimates varied between -77 mm and 0 mm at Lake A and between -58 mm and 42 mm at Lake B, respectively. The opposite water flow directions between the lake and the supra-permafrost aquifer in the dry year of 2012 and in the wet year of 2013 indicates that

there was a considerable supra-permafrost discharge before freezing up of the active layer in the wet year.

Figure 5 compares the seasonal contributions of the supra-permafrost discharge of the lakes. In the ice-free seasons, the supra-permafrost discharge contributed a mean of 177% that of the direct precipitation for lake volume at Lake A, 168% at Lake B. The mean ratio of the inputs of the supra-permafrost discharge and direct precipitation are both over 150%. In the ice-cover seasons, the contribution of the supra-permafrost discharge to the change of lake water volume varied between 22% and 0 from 2012 to 2013 at Lake A and between 18% and -20% at Lake B.

#### **4.2 Major factors affecting the seasonal supra-permafrost discharge**

In the ice-free season, the supra-permafrost water generates from precipitation and active layer thaw, and the supra-permafrost discharge to lakes is also influenced by factors like precipitation intensity, time, and the freeze-thaw process. Figure 6 compares the normalized accumulative rainfall and supra-permafrost discharge for the three ice-free seasons in 2012, 2013, and 2014. A fill-spill pattern (Spence and Woo, 2003) is generally summarized as follows. First of all, the supra-permafrost discharge emerges when saturated layer forms in the thawed supra-permafrost aquifer. As shown in Fig. 4c, a saturated layer in the supra-permafrost aquifer normally formed in early July when the thawing front reached a water level about 1.4 m below surface. When the supra-permafrost water level is elevated over this threshold by an intense rainfall event, and the supra-permafrost discharge will increase nonlinearly. Finally, the discharge decreases and the flow direction is even reserved for some cases in the late autumn. Generally, most of the large supra-permafrost discharges occur with the intensive rainfall events, but the relationship between the rainfall and the supra-permafrost discharge is also affected by the open surface area of the lake system and water level in the

active layer. As a sink of a local closed system, Lake A did not spill as Lake B with sharp recessions after intensive rainfall events, since intermittent runoff happened at Lake B when the water level is over a certain height. In addition, the dramatic drop of accumulative flux in 2014 at Lake A happened at the end of May, when the lake was connected to the supra-permafrost aquifer by active layer thaw with a higher water level than 1.4 m.

In the ice-cover season, the seasonal supra-permafrost discharge was controlled by the relationship of water exchange between the supra-permafrost aquifer and the lake during the active layer freeze. Considering the coarse soils, the influence of the freezing suction on the supra-permafrost water level decrease is thought to be negligible. The regional supra-permafrost water drained via the saturated zone until frozen up (e.g., zone 1 and zone2). After a dry ice-free season, water heads of the supra-permafrost aquifer and the lake are both low and drained consistently. The lake spilling led to a negative  $\Delta L$  value in 2012. In contrast, after a wet ice-free season, the supra-permafrost aquifer still filled the lake and resulted in a positive  $\Delta L$  value in 2013.

In general, the dramatic change of the lake water volume is dominated by the precipitation change which causes supra-permafrost discharge. The response of the lake water volume to different weather conditions is illustrated in Fig. 7. For a dry weather, the lake is mainly filled by the supra-permafrost discharge in the ice-free season and conversely recharge the supra-permafrost aquifer in the ice-cover season. However, for a wet weather, the supra-permafrost discharge to the lake increase dramatically in both seasons, and leads to a larger water volume. Furthermore, the warming climate will not only affect the thickness of the active layer, but also lead to the formation of a talik which will likely increase the supra-permafrost discharge in the ice-cover season. The conceptual permafrost mechanisms related to the supra-permafrost discharge in Fig. 7 is expected to be more common in the near future.

### 4.3 Implications for the recent changes of the high-altitude lakes

Given such an important role of the precipitation-induced supra-permafrost discharge in the lake water dynamics, identifying the relationship between the supra-permafrost discharge and precipitation is essential for understanding the consequence of precipitation change. Figure 8 shows the monthly and seasonal observations of the supra-permafrost discharge and precipitation for both lakes, and exponential functions were used for fitting. The dispersive distribution in Fig. 8a is mainly related to the active layer thawing. As shown in Fig. 6c and 6e, the changes of the supra-permafrost discharge at the beginning are not controlled by precipitation but the active layer thawing. Besides, limited by the short period of seasonal observations in Fig. 8b, the relationship might be less representative. Nevertheless, the supra-permafrost discharge increases nonlinearly with precipitation increase. Thus, the precipitation-runoff function would be a key factor in predicting supra-permafrost discharge in response to precipitation increase. Furthermore, the other factors like active layer thaw and permafrost distribution also affect the runoff coefficient along with permafrost degradation in a longer period.

From three-year intensive field measurements, this study exemplifies the importance of subsurface runoff to the water balance of a simple thermokarst lake system at high altitude (>4400m a.s.l.). Because of a relatively short period of observations, verifying the decadal change of the thermokarst lakes is not viable. However, the three-year measurements provide data for us to propose a nonlinear relationship between precipitation and supra-permafrost discharge which can be important for the recent high-latitude lake growth on the QTP. The above results might be also valid for the large lakes in other permafrost environments, although we need to further understand their hydrological processes. Therefore, future studies should further investigate the amplified subsurface runoff due to precipitation increase which

many current hydrological models for the large lakes in the permafrost catchments have not well considered.

## 5 Summary and conclusions

In this study, we have used different field observations between 2012 and 2014 to investigate the hydrological dynamics of the two shallow thermokarst lakes on the northeastern QTP.

From these, we have identified that the supra-permafrost discharge can be a specific control factor of the QTP lake expansion. Our findings are summarized as follows;

- (1) In the cold and arid QTP, our three-year water budget results show that the annual vertical water input to the thermokarst lake system is -360.5 mm. Therefore, in this relatively closed system, the precipitation-controlled supra-permafrost discharge is the main control of lake volume for the investigated thermokarst lakes in the ice-free season, instead of direct precipitation input to the lake.
- (2) Seasonal lake water volume is affected by the supra-permafrost discharge, apart from the vertical input. In the ice-free season, the supra-permafrost discharge contributes the lake volume with a mean ratio of over 170% of the precipitation. During the ice-covered season, the connectivity between the lake and the permafrost reduces. As a result, the lake volume change has less contribution from the supra-permafrost discharge, and the contribution can be negative in some cases. Our estimation is between -20% and 22% for the lake volume change due to the supra-permafrost discharge in the ice-covered season.
- (3) Our results provide evidence that the recent lake expansion is linked with the increasing precipitation-controlled supra-permafrost discharge. A precipitation-runoff function was preliminarily identified in which the supra-permafrost discharge nonlinearly increased with precipitation increase. This could be a key factor in

predicting the water storage variation of the thermokarst lakes in response to precipitation increase, apart from the factor of permafrost change.

Based on the above precipitation-runoff mechanism, we suggest that the nonlinear increase of the precipitation-controlled supra-permafrost discharge may be not negligible in contributing the recent lake growth on the QTP. In addition to only looking at inputs (e.g., precipitation and river discharge) in the current prevailing studies, we should pay more attention to the supra-permafrost discharge. Apart from the factors like thickening active layers and increased precipitation, the precipitation-runoff mechanism in permafrost catchments is another important control factor for lake water storage variation at a decadal scale. In light of the complex hydrological system of large lakes, further verification of the insights from the small thermokarst lakes is needed for interpreting the recent lake expansion.

### **Acknowledgments**

We would like to thank Dr. Lei Guo and Xinbing Wang for field assistance. This study was partly funded by the National Natural Science Foundation of China grants: 41771262, 41171059 and 41401088). Dr. K. P. Chun is supported by the Hong Kong Baptist University Faculty Research Grants (FRG2/16-17/082, FRG1/17-18/005).

### **References**

Allen, R.G., Pereira, L.S., Raes, D., Smith, M., 1998. Crop Evapotranspiration-Guidelines for Computing Crop Water Requirements-FAO Irrigation and Drainage Paper 56. United Nations Food and Agriculture Organization, Rome, Italy.

- Arp, C.D., Jones, B.M., Urban, F.E., Grosse, G., 2011. Hydrogeomorphic processes of thermokarst lakes with grounded-ice and floating-ice regimes on the Arctic coastal plain, Alaska. *Hydrol. Process.* doi:10.1002/hyp.8019.
- Bowling, L.C., Kane, D.L., Gieck, R.E., Hinzman, L.D., Lettenmaier, D.P., 2003. The role of surface storage in a low-gradient Arctic watershed. *Water Resour. Res.* 39(4), 1087.
- Brocca, L., Massari, C., Ciabatta, L., Moramarco, T., Penna, D., Zuecco, G., Pianezzola, L., Borga, M., Matgen, P., Martínez-Fernández, J., 2015. Rainfall estimation from in situ soil moisture observations at several sites in Europe: an evaluation of the SM2RAIN algorithm. *J. Hydrol. Hydromech.* 63, 201–209.
- Brocca, L., Moramarco, T., Melone, F., Wagner, W., 2013. A new method for rainfall estimation through soil moisture observations. *Geophys. Res. Lett.* 40, 853–858, doi:10.1002/grl.50173.
- Brock, B.E., Wolfe, B.B., Edwards, T.W.D., 2007. Characterizing the hydrology of shallow floodplain lakes in the Slave River Delta, NWT, Canada, using water isotope tracers. *Arct. Antarct. Alp. Res.* 39 (3), 388–401.
- Brunt, D., 1952. *Physical and dynamical meteorology*, 2nd ed., Univ. Press, Cambridge, pp. 428.
- Burman, R.D., Jensen, M.E., Allen, R.G., 1987. Thermodynamic factors in evapotranspiration. In: James, L.G. and M.J. English (editors), *Proc. Irrig. and Drain. Spec. Conf.*, ASCE, Portland, Ore., pp. 28-30.
- Burn, C.R., 2002. Tundra lakes and permafrost, Richards Island, western Arctic coast, Canada. *Can. J. Earth Sci.* 39, 1281–1298.

- Connon, R.F., Quinton, W.L., Craig, J.R., Hayashi, M., 2014. Changing hydrologic connectivity due to permafrost thaw in the lower Liard River valley, NWT, Canada. *Hydrol. Process.* 28, 4163–4178. doi:10.1002/hyp.10206.
- Efron, B., Tibshirani, R.J., 1993. *An Introduction to the Bootstrap*, Chapman and Hall, New York.
- Finch, J., Calver, A., 2008. *Methods for the quantification of evaporation from lakes*, Prepared for the World Meteorological Organization Commission of Hydrology, CEH Wallingford, UK.
- Finch, J.W., Hall, R.L., 2001. *Estimation of open water evaporation*. R&D Project W6043, Environment Agency.
- Gibson, J. J., 2001. Forest-tundra water balance signals traced by isotopic enrichment in lakes. *J. Hydrol.* 251, 1–13.
- Harris, S.A., 2002. Causes and consequences of rapid thermokarst development in permafrost or glacial terrain. *Permafrost Periglac.* 13, 237–242.
- Hayashi, M., van der Kamp, G., 2007. Water level changes in ponds and lakes: the hydrological processes. In: Johnson E, Miyanishi K (eds) *Plant disturbance ecology*. Academic, Burlington.
- Kaeab, A., Haeberli, W., 2001. Evolution of a high-mountain thermokarst lake in the Swiss Alps. *Arctic, Antarctic Alpine Res.* 33, 385–390.
- Kling, G.W., Kipphut, G.W., Miller, M.C., 1991. Arctic lakes and streams as gas conduits to the atmosphere: implications for tundra carbon budgets. *Science* 251, 298–301.

- Kouraev, A.V., Semovski, S.V., Shimaraev, M.N., Mognard, N.M., Légresy, B., Remy, F., 2007. Observations of Lake Baikal ice from satellite altimetry and radiometry. *Remote Sens. Environ.* 108(3), 240–253.
- Kuchment, L.S., Gelfan, A.N., 1996. The determination of the snowmelt rate and the meltwater outflow from a snowpack for modelling river runoff generation. *J. Hydrol.* 179, 23–36.
- Kurylyk, B.L., Hayashi, M., Quinton, W.L., McKenzie, J.M., Voss, C.I., 2016. Influence of vertical and lateral heat transfer on permafrost thaw, peatland landscape transition, and groundwater flow. *Water Resour. Res.* 52, 1286–1305. doi:10.1002/2015WR018057.
- Labrecque, S., Lacelle, D., Duguay, C.R., Lauriol, B., Hawkings, J., 2009. Contemporary (1951–2001) evolution of lakes in the Old Crow Basin, Northern Yukon, Canada: remote sensing, numerical modeling, and stable isotope analysis. *Arctic* 62(2), 225–238.
- Lei, Y., Yao, T., Bird, B.W., Yang, K., Zhai, J., Sheng, Y., 2013. Coherent lake growth on the central Tibetan Plateau since the 1970s: Characterization and attribution. *J. Hydrol.* 483, 61–67.
- Li, L., Li, F., Guo, A., Zhu, X., 2006. Study on the climate change trend and its catastrophe over "Sanjiangyuan" region in recent 43 years (in Chinese). *Journal of Natural Resources* 21, 79–85.
- Lin, Z., Niu, F., Xu, Z., Xu, J., Wang, P., 2010. Thermal regime of a thermokarst lake and its influence on permafrost, Beiluhe basin, Qinghai-Tibet Plateau. *Permafrost Periglac.* 21, 315–324, doi:10.1002/ppp.692.
- Liston, G.E., Sturm, M., 2004. The role of winter sublimation in the Arctic moisture budget. *Nord. Hydrol.* 35(4), 325–334.

- Livingstone, D., 1999. Ice break-up on southern Lake Baikal and its relationship to local and regional air temperatures in Siberia and the North Atlantic Oscillation. *Limnol. Oceanogr.* 44, 1486–1497.
- McNamara, J.P., Kane, D.L., Hinzman, L.D., 1998. An analysis of stream flow hydrology in the Kuparuk River Basin, Arctic Alaska: A nested watershed approach. *J. Hydrol.* 206, 39–57.
- McMahon, T.A., Peel, M.C., Lowe, L., Srikanthan, R., McVicar, T.R., 2013. Estimating actual, potential, reference crop and pan evaporation using standard meteorological data: a pragmatic synthesis. *Hydrol. Earth Syst. Sci.* 17, 1331–1363.
- Murray, F.W., 1967. On the computation of saturation vapor pressure. *J. Appl. Meteor.* 6, 203–204.
- Niu, F., Lin, Z., Liu, H., Lu, J., 2011. Characteristics of thermokarst lakes and their influence on permafrost in Qinghai-Tibet Plateau. *Geomorphology* 132, 222–233.
- Pan, X., You, Y., Roth, K., Guo, L., Wang, X., Yu, Q., 2014. Mapping permafrost features that influence the hydrological processes of a thermokarst lake on the Qinghai-Tibet Plateau, China. *Permafrost Periglac.* 25, 60–68. doi:10.1002/ppp.1797.
- Pan, X., Li, Y., Yu, Q., Shi, X., Yang, D., Roth, K., 2016. Effects of stratified active layers on high-altitude permafrost warming: a case study on the Qinghai–Tibet Plateau. *The Cryosphere* 10, 1591–1603.
- Pohl, S., Marsh, P., Onclin, C., Russell, M., 2009. The summer hydrology of a small upland tundra thaw lake: implications to lake drainage. *Hydrol. Process.* 23, 2536–2546.
- Pomeroy, J.W., Essery, R.L.H., 1999. Turbulent fluxes during blowing snow: field test of model sublimation predictions. *Hydrol. Process.* 13, 2963–2975.

- Quinton, W.L., Marsh, P., 1999. A conceptual framework for runoff generation in a permafrost environment. *Hydrol. Process.* 13(16), 2563–2581.
- Rouse, W.R., Oswald, C.M., Binyamin, J., 2003. Interannual and seasonal variability of the surface energy balance and temperature of central Great Slave Lake. *J. Hydrometeorol.* 4, 720–730.
- Smith, L.C., Sheng, Y., MacDonald, G.M., Hinzman, L.D., 2005. Disappearing Arctic Lakes. *Science* 308, 1429.
- Song, C., Huang, B., Richards, K., Ke, L., Phan, V.H., 2014. Accelerated lake expansion on the Tibetan Plateau in the 2000s: Induced by glacial melting or other processes? *Water Resour. Res.* 50, 3170–3186. doi:10.1002/2013WR014724.
- Spence, C., Woo, M.K., 2003. Hydrology of subarctic Canadian shield: soil- filled valleys. *J. Hydrol.* 279, 151–166.
- Sturm, M., Liston, G.E., Benson, C.S., Holmgren, J., 2001. Characteristics and growth of a snowdrift in arctic Alaska. *Arctic, Antarctic Alpine Res.* 33(3), 319–332.
- Tetens, O., 1930. Uber einige meteorologische Begriffe. *z. Geophys.* 6, 297-309.
- Turner, K.W., Wolfe, B.B., Edwards, T.W.D., 2010. Characterizing the role of hydrological processes on lake water balances in the Old Crow Flats, Yukon Territory, Canada, using water isotope tracers. *J. Hydrol.* 386, 103–117.
- Walter, K.M., Zimov, S.A., Chanton, J.P., Verbyla, D., Chapin, F.S., 2006. Methane bubbling from Siberian thaw lakes as a positive feedback to climate warming. *Nature* 443, 71–75.
- Walvoord, M.A., Kurylyk, B.L., 2016. Hydrologic impacts of thawing permafrost – a review. *Vadose Zone J.* 15(6). doi: 10.2136/vzj2016.01.0010.

Wang, L., Li, X., Zhou, J., Liu, W., Yang, K., 2014. Hydrological modelling over the Tibetan Plateau: current status and perspective. *Advances in Earth Science* 2014(6): 674–682(in Chinese).

van Everdingen, R.O., 2005. Multi-Language Glossary of Permafrost and Related Groundice Terms, National Snow and Ice Data Center/World Data Center for Glaciology, Boulder, available at: <http://nsidc.org/fgdc/glossary>.

Vincent, W.F., Hobbie, J.E., 2000. Ecology of Arctic lakes and rivers. In: Nuttal, M, Callaghan, T.V. (Eds.), *The Arctic: Environment, People, and Policy*. Overseas Publishers Association, Amsterdam, pp. 197–274.

Yang, Y., Wu, Q., Yun, H., Jin, H., Zhang, Z., 2016. Evaluation of the hydrological contributions of permafrost to the thermokarst lakes on the Qinghai – Tibet Plateau using stable isotopes. *Global and Planet. Change* 140, 1–8.

You, Y., Yu, Q., Pan, X., Wang, X., Guo, L., 2017a. Geophysical imaging of permafrost and talik configuration beneath a thermokarst lake. *Permafrost Periglac.*, doi: 10.1002/ppp.1938.

You, Y., Yu, Q., Pan, X., Wang, X., Guo, L., Wu, Q., 2017b. Thermal effects of lateral supra-permafrost water flow around a thermokarst lake on the Qinghai-Tibet Plateau, *Hydrol. Process.* 31(13), 2429-2437.

Zhou, J., Wang, L., Zhang, Y., Guo, Y., Li, X., Liu, W., 2015. Exploring the water storage changes in the largest lake (Selin Co) over the Tibetan Plateau during 2003–2012 from a basin-wide hydrological modeling. *Water Resour. Res.* 51, 8060–8086, doi:10.1002/2014WR015846.

Zhou, Y., Guo, D., Qiu, G., Cheng, G., Li, S., 2000. Geocryology in China [in Chinese], Science Press, pp. 1–34.

Zimov, S.A., Voropaev, Y.V., Semiletov, I.P., et al., 1997. North Siberian lakes: a methane source fueled by pleistocene carbon. *Science* 277, 800–802.

ACCEPTED MANUSCRIPT

Table 1 Additional atmospheric formulas for Eq. (4).

1. Slope vapor pressure curve,  $\Delta$  [kPa  $^{\circ}\text{C}^{-1}$ ]

$$\Delta = \frac{4098 \left[ 0.6108 e^{\left( \frac{17.27 T_{mean}}{T_{mean} + 237.3} \right)} \right]}{(T_{mean} + 237.3)^2} \quad (\text{Tetens, 1930; Murray, 1967})$$

$T_{mean}$ : the daily mean air temperature, [ $^{\circ}\text{C}$ ].

2. Psychrometric constant, [kPa  $^{\circ}\text{C}^{-1}$ ]

$$\gamma = \frac{c_p P_a}{\epsilon \lambda}$$

$P_a$ : the atmospheric pressure, [kPa]

(Brunt, 1952)

$c_p$ : specific heat at constant pressure,  $1.013 \times 10^{-3}$ , [MJ  $\text{kg}^{-1} \text{ } ^{\circ}\text{C}^{-1}$ ]

$\lambda$ : latent heat of vaporization, 2.45, [MJ  $\text{kg}^{-1}$ ]

$\epsilon$ : ratio molecular weight of water vapor/dry air, 0.622

3. Atmospheric pressure at the elevation  $z_e$  (4445 m a.s.l.),  $P_a$  [kPa]

$$P_a = \left( \frac{293 - 0.0065 z_e}{293} \right)^{5.26} \quad (\text{Burman et al., 1987})$$

4. Daily saturation vapor pressure,  $e_s$  [kPa]

$$e_{T_a} = 0.6108 \exp\left(\frac{17.27 T_a}{T_a + 237.3}\right), \text{ and } e_s = \frac{e_{(T_{\max})} + e_{(T_{\min})}}{2} \quad (\text{Tetens, 1930})$$

$T_{\max}$  and  $T_{\min}$ : daily extremes of air temperature, [ $^{\circ}\text{C}$ ]

5. Daily actual vapor pressure,  $e_a$ , [kPa]

$$e_a = \frac{e_{(T_{\max})} \frac{RH_{\min}}{100} + e_{(T_{\min})} \frac{RH_{\max}}{100}}{2},$$

where,  $H_{\max}$  and  $H_{\min}$ : daily extremes of relative humidity, [%]

Table 2 Calculated components of seasonal water budget (mm),  $P$ : precipitation,  $E$ : evaporation,  $\Delta L$ : supra-permafrost water flux,  $\Delta S$ : lake water volume change.

Seasons	$P$	$E$	Lake A		Lake B	
			$\Delta S$	$\Delta L$	$\Delta S$	$\Delta L$
Ice-free '12* (Jul. 3 - Oct. 14)	124±27	224±35	94±5	194±44	140±5	238±44
Ice-cover '13/14 (Oct. 15- Apr. 18)	0	271±31	-348±5	-77±31	-329±5	-58±31
Ice-free '13 (Apr. 19 - Oct. 15)	292±61	457±67	502±5	667±91	341±5	506±91
Ice-cover '13/14 (Oct. 16 - May 4)	0	249±20	-249±5	0±20	-207±5	42±20
Ice-free '14 (May 5 - Oct. 6)	245±51	348±52	257±5	360±73	239±5	342±73

\* Incomplete period.

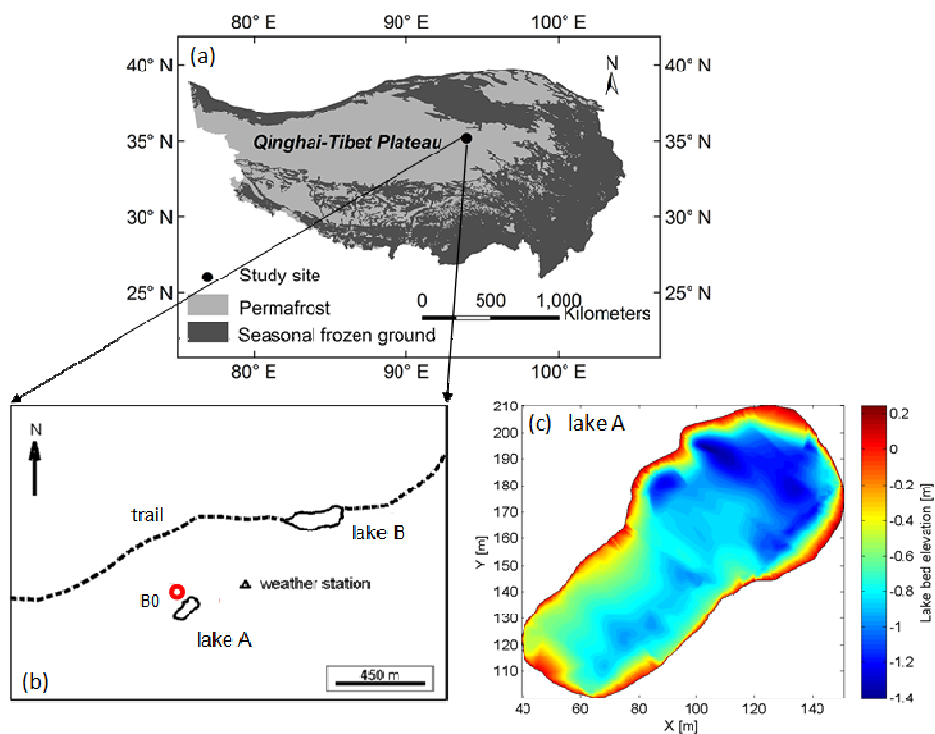


Figure 1. Location of two lakes and instrumentation at the study site. (a) Permafrost distribution of the Qinghai-Tibet Plateau (modified from You et al., (2017)). (b) Distribution of two lakes, water level borehole on the bank (B0), and soil-weather monitoring station. (c) Lake bed topography of Lake A (modified from Pan et al., (2014)).

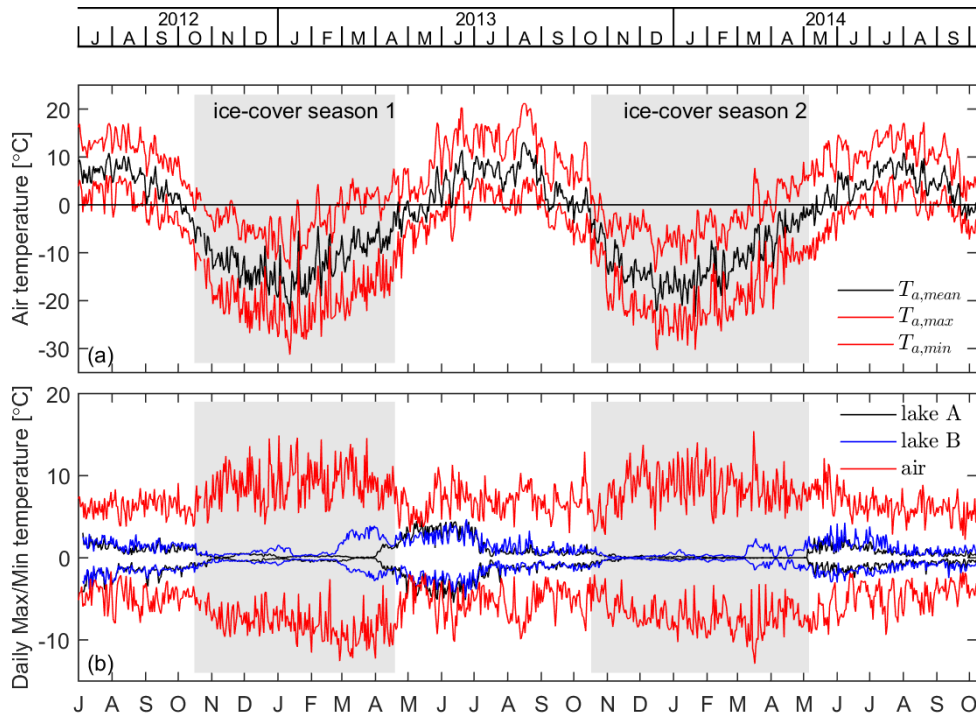


Figure 2. Identification of ice-cover seasons (gray areas) from time series of air temperature, lake bottom temperature observations. (a) The daily mean, maximum and minimum values of air temperature ( $T_{a,mean}$ ,  $T_{a,max}$ , and  $T_{a,min}$ ). (b) Contrast features of the daily dynamic ranges of air temperature, lake bottom temperatures (Lake A and Lake B) relative to the daily means between ice-free seasons and ice-cover seasons.

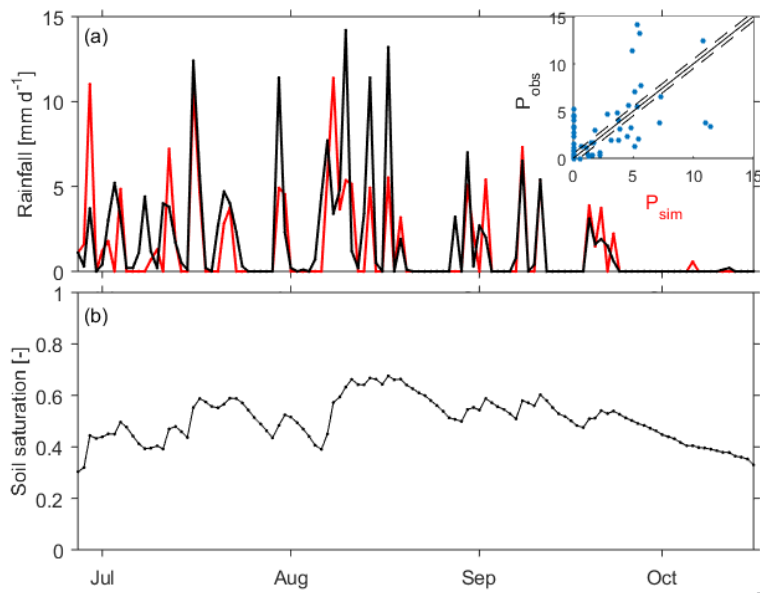


Figure 3. Comparison of observed and estimated daily rainfall during the ice-free season in 2012. (a)  $P_{\text{obs}}$  is the observed rainfall and  $P_{\text{sim}}$  is estimated using the Eq. (9). The dashed lines in the upper corner stand for a standard deviation of  $0.35 \text{ mm d}^{-1}$ . (b) The daily averaged soil saturation of the top 10 cm.

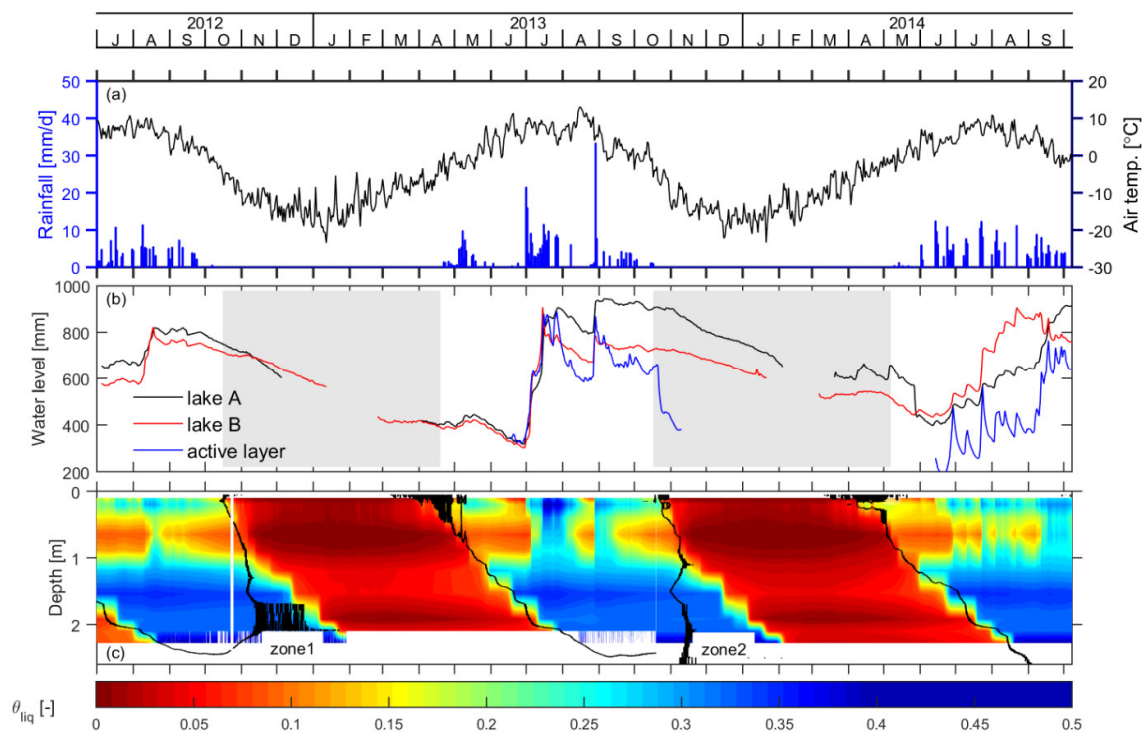


Figure 4. Fluctuation of the major variables in thermokarst lake hydrology in 2012-2014. (a) Daily mean air temperature and estimated rainfall excluding solid precipitation. (b) Lake water dynamics at the Lake A and the Lake B; dashed lines show the drop of water-level in ice-cover seasons (gray color). (c) Unfrozen soil water dynamics ( $\theta_{liq}$ ) and thawing front (black curve) in the monitoring profile at the weather station (Fig. 1b). Zone 1 and Zone 2 shows the potential supra-permafrost water discharge at the beginning of the ice-cover seasons.

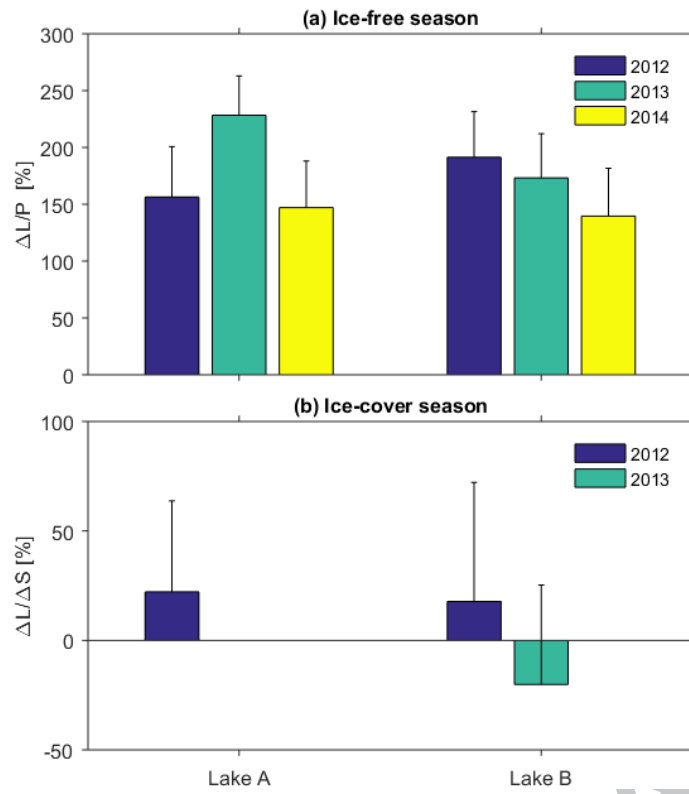


Figure 5. The seasonal contributions of supra-permafrost water to the lake water volume change in 2012-2014.  $P$ : precipitation,  $\Delta L$ : the supra-permafrost discharge, and  $\Delta S$ : the lake water volume change.

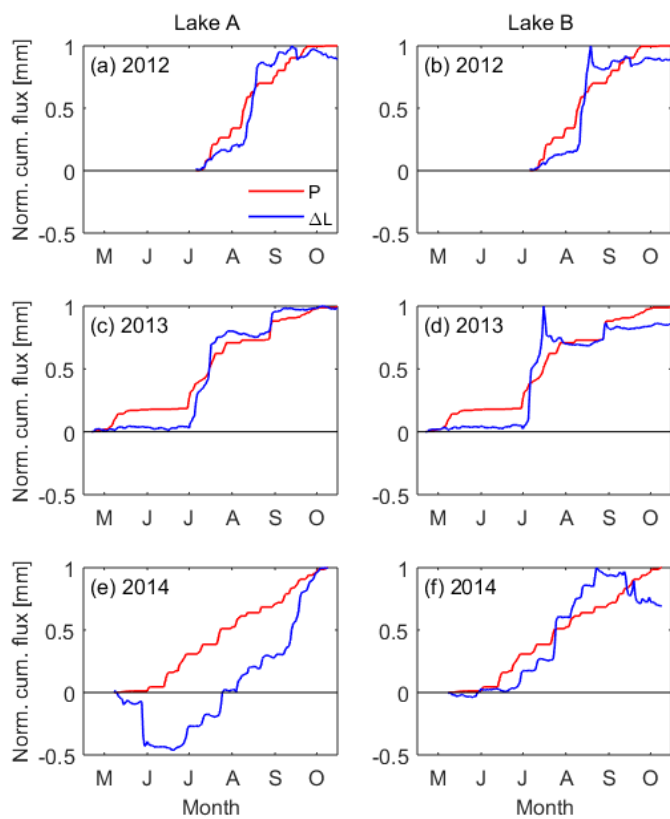


Figure 6. Temporal variations of the relationship between rainfall and supra-permafrost discharge to the two lakes in the ice-free seasons of 2012, 2013, and 2014.  $P$  and  $\Delta L$  are the normalized cumulative precipitation and supra-permafrost discharge, respectively.

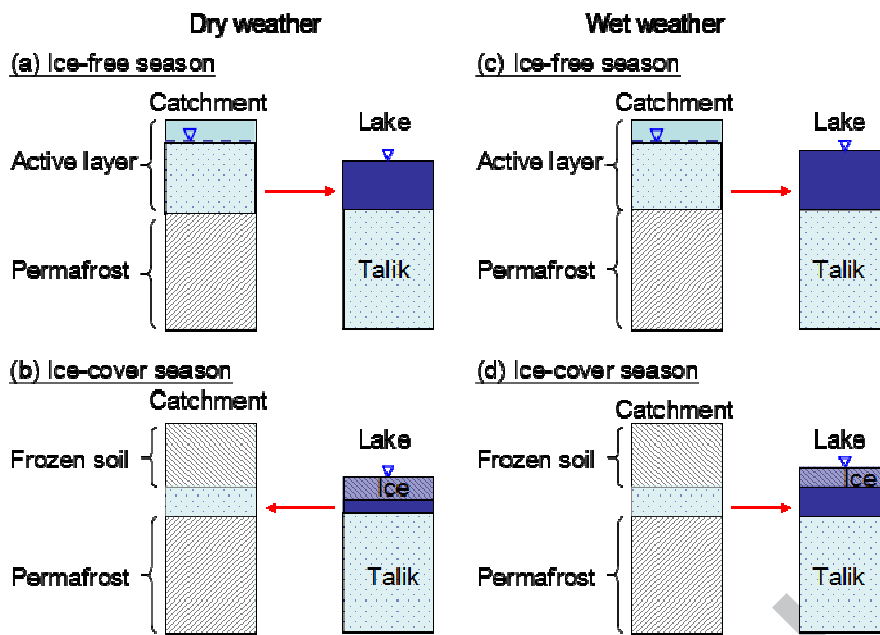


Figure 7. Schematic models of seasonal water exchange between the catchment permafrost aquifer and the thermokarst lake at different weather conditions. The left panel: the discharge by the rainwater induced supra-permafrost water to the lake in the ice-free season is partially offset by the catchment supra-permafrost discharge in the ice-cover season at a dry weather condition. The right panel: the lake is discharged in both seasons by the catchment supra-permafrost aquifer at a wet weather condition.

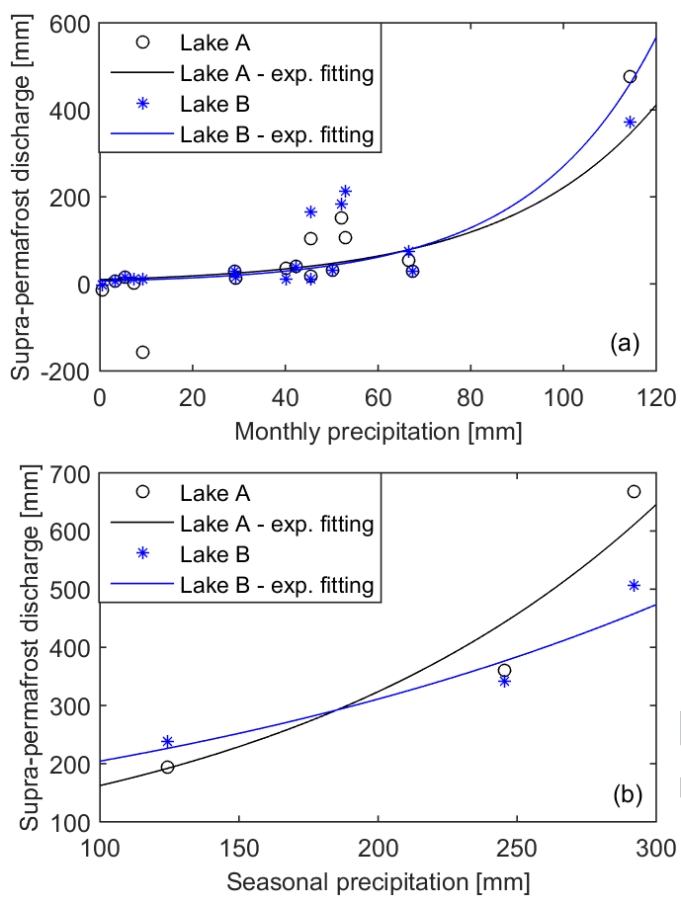


Figure 8. Relationships between the supra-permafrost discharge and the precipitation at the two lakes. (a) monthly, and (b) seasonally.

### 1.1 Highlights

- The precipitation-induced supra-permafrost discharge plays an important role in the water balance of thermokarst lakes on the Qinhai-Tibet Plateau.
- The contribution of supra-permafrost discharge to lake water balance can increase nonlinearly with precipitation, based on an exponential precipitation- subsurface runoff relation.
- The results provide a novel conceptual model for interpreting the recent lake growth on the Tibetan Plateau.

ACCEPTED MANUSCRIPT